51st AIAA/ASME/ASCE/AHS/ASC Structures, Structural Dynamics, and Materials Conference
 18th
12 - 15 April 2010, Orlando, Florida

AIAA 2010-2706

Homogenization of Plates with Microsctructure and Application to Corrugated Core Sandwich Panels

Anurag Sharma[1] Bhavani V. Sankar[2] Raphael T. Haftka[3]
Department of Mechanical and Aerospace Engineering, University of Florida,
PO Box 116250, Gainesville, FL 32611-6250

Current thermal protection systems (TPS) in hypersonic vehicles do not carry significant loads. One potential method of saving weight is to have a load-bearing TPS that performs some structural functions. One such concept, the Integrated Thermal Protection System (ITPS), uses a corrugated-core sandwich structure. Design-optimization of an ITPS requires thousands of three-dimensional high-fidelity simulations, which is very expensive. In this paper we develop a finite element based homogenization procedure for predicting the equivalent stiffness and strength properties of the ITPS. Micromechanical analysis is possible due to the presence of a repeating unit-cell. The unit cell is discretized with plate finite elements, and periodic boundary conditions are imposed between opposite end-faces of the unit cell. The derivation of the periodic boundary conditions is presented. The equivalent stiffness properties, the extensional stiffness matrix [*A*], coupling stiffness matrix [*B*], bending stiffness [*D*], and the transverse shear stiffness terms A_{44} and A_{55} are obtained using the micromechanics procedures. The plate deflection under uniform pressure compares well with that from the three-dimensional finite element analysis. The efficacy of the procedures is demonstrated by studying the effects of web angle on the plate stiffness and deflection.

Nomenclature

a	=	panel length, x direction
b	=	panel length, y direction
d	=	height of the sandwich panel (centerline to centerline)
t_T	=	top face sheet thickness
t_B	=	bottom face sheet thickness
t_C	=	web thickness
θ	=	angle of web inclination
L	=	length of the ITPS panel
n	=	number of unit cells in the panel
$2p$	=	unit cell length
$F_i^{(m)}$	=	nodal force in the finite element model
N_i, M_i	=	force and moment resultant
ε_o	=	mid-plane strain
κ	=	curvature
u,v,w	=	displacement in the x, y and z directions
u_0, v_0, w_0	=	mid-plane plate displacements
ψ_x, ψ_y	=	plate rotations

[1]Graduate Student & Corresponding Author (anurag46@ufl.edu)
[2]Newton C. Ebaugh Professor, Associate Fellow AIAA. (sankar@ufl.edu)
[3]Distinguished Professor, Fellow AIAA (haftka@ufl.edu)

I. Introduction

Reducing the cost of launching a space vehicle is one of the vital requirements of the space industry. There is a major demand for low-cost space access from the government and industries. The government launches satellites for weather, military communication, scientific, and reconnaissance purposes. If use of space is to become routine, future space vehicles must become fully reusable, have greater operational flexibility, and have a lower operating cost than the current space vehicles like the Space Shuttle. Reducing the cost of delivering a pound of payload into space by an order of magnitude is one of NASA's objectives in achieving their low cost and reliable space access. The space vehicle's TPS (Thermal Protection System) is one of the most expensive and critical systems of the vehicle. The TPS protects the vehicle structure traveling at hypersonic speeds through a planetary atmosphere from damage due to aerodynamic heating. It occupies huge acreage on vehicle exteriors and accounts for a significant part of the launch weight. Metallic TPS was considered as the primary heat shield for the Space Shuttle. Blosser [1,2] designed an advanced-adapted, robust, metallic, operable, reusable (ARMOR) TPS concept. However, the ARMOR TPS's load bearing capabilities are limited, and large in-plane loads cannot be accommodated under this design.

Selection of the optimum TPS for a particular space vehicle is a challenging task that requires considerations of weight, operability, reusability, maintenance, durability, initial cost, life-cycle cost, and compatibility. The common feature between the Apollo, Space Shuttle, and X-33 Venture Star™ TPS concepts was that their TPS was an add-on to the vehicle's outer structure. The tiles coefficient of thermal expansion (CTE) is less than the vehicle structure CTE which is aluminum. As a result of that incompatibility, direct mounting of the TPS to the structure was not possible. The add-on feature created this incompatibility problem between the thermal structure and the load-bearing structure of the vehicle as well as an increase in maintenance. These various TPS concepts were also not load bearing members; they were purely thermal structures. Fasteners, frames, and support brackets contributed to the overall weight of the TPS and the TPS as an add-on feature added mass to the total vehicle weight and hence the cost [3].

One potential way of saving weight is to have a load-bearing TPS that performs structural functions. One such concept called the Integrated Thermal Protection System (ITPS) uses a corrugated-core sandwich structure. An ITPS is a sandwich panel composed of two thin faces separated by a corrugated core structure which can be of homogeneous materials such as metals or orthotropic materials such as composite laminates. The sandwich panel is composed of several unit cells placed adjacent to each other. The empty space in the corrugated core will be filled with a non load-bearing insulation such as Safill®.

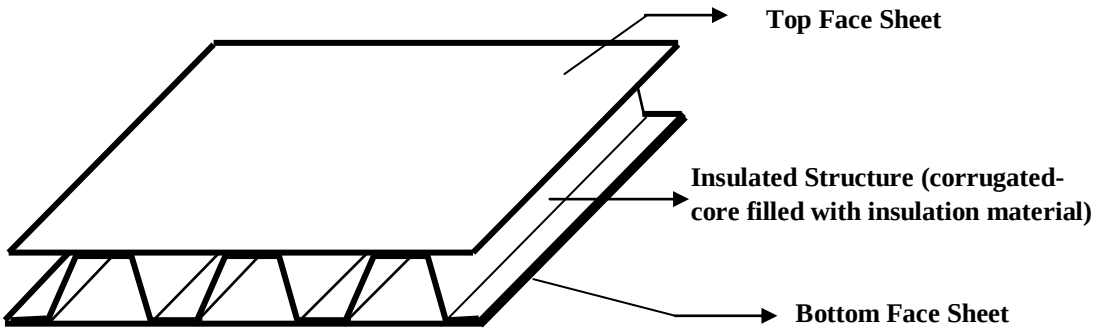

Figure 1. A corrugated-core sandwich structure concept for Integrated Thermal Protection System (ITPS).

This sandwich panel has high stiffness due to thin flat faces when compared to the low average stiffness of the thick core. Sandwich constructions are frequently used because of their high bending stiffness-to-weight ratio. The high bending stiffness is the result of the distance of the face sheets from the neutral axis. The face sheets support the major portion of the in-plane loads. The core helps stabilize the face sheets and supports the shear loads through the thickness. The corrugated core keeps the face sheets apart and stabilizes them by resisting vertical deformations, transverse shear strains, curvature in the longitudinal direction, and enables the structure to acts as a single thick

plate. Unlike a soft honeycomb core, a corrugated core resists bending and twisting in addition to vertical shear [4]. All these characteristics make corrugated sandwich structures ideal for aviation, aerospace, civil engineering, and marine applications, where weight and stiffness are important design drivers.

Ideally, we can homogenize the sandwich panel as a continuous, orthotropic plate. This would require the prediction of the effective (macroscopic) properties of the sandwich panel from the constituent material (microscopic) characteristics. This is possible if there is a representative volume element (RVE) or a unit cell that repeats itself throughout the volume of the composite. The unit cell can be considered as the smallest building block, such that the whole structure can be created by assembling the unit cell in all dimensions. This prediction of the effective macroscopic properties from the constituent material characteristics is known as micromechanics [5].

Various researchers such as Lok et al [6,7] and Valdevit et al [8] analyzed metallic truss-core sandwich panels subjected to mechanical loadings. Biancolini [9] derived the equivalent stiffness properties of corrugated boards by performing static condensation of the stiffness matrix obtained using the finite element (FE) model of the full panel. Buannic et al. [10] used asymptotic expansion based analytical method for deriving the equivalent properties of corrugated panel. Martinez et al [11,12] developed an analytical model of the ITPS based on homogenization of the panel for calculating the various stiffnesses using strain energy approach. The analytical model for homogenizing the ITPS as an orthotropic plate was based on many simplifying assumptions regarding the deformation of the structure. The analytical model resulted in a reasonably good estimate of stiffness properties, e.g., *A*, *B* and *D* matrices for certain material combination; however it varied considerably for unsymmetrical material properties and thickness. Also, the transverse shear stiffness properties, A_{44} and $A_{55,}$ differed significantly as the homogenized plate could not faithfully represent the local behavior of the ITPS. Further for widely varying geometries and different material properties for the top face sheet (TFS), bottom face sheet (BFS) and the web, the discrepancies will be even more and hence a finite element method based homogenization procedure was developed to obtain the equivalent plate properties.

The main objective of the paper is to determine the equivalent stiffness properties of the ITPS panel using a finite element model. Six linearly independent deformations are applied to the unit cell using the periodic boundary conditions. The derivations and the assumptions used in deriving the six periodic boundary conditions are also discussed. The extensional stiffness matrix [*A*], coupling stiffness matrix [*B*], bending stiffness [*D*], and the transverse shear stiffness terms, A_{44} and $A_{55,}$ are calculated using a finite element model by applying these periodic boundary condition. These equivalent stiffness properties are then applied to the plate finite element model and the maximum deflection under uniform pressure is compared with the three dimensional ITPS panel analysis. A sensitivity analysis of the stiffness properties with respect to the change in web inclination is also done.

In Section II we identify the geometric variables and the material properties for the ITPS panel. In Section III, we give the derivation of the periodic boundary conditions and the basic assumptions undertaken while deriving these boundary conditions. In Section IV, we provide the derivation of the transverse shear stiffness properties, A_{44} and A_{55}, using FE approach. Finally, in Section V we discuss the results and the limitations of the FE based micromechanics approach.

II. Geometric Variables and Material Properties

The geometry of the ITPS structure with corrugated-core design is shown in Fig. 2. This geometry can be completely described using the following seven geometric variables:

1. Thickness of top face sheet, t_T,
2. Thickness of webs, t_W,
3. Thickness of bottom face sheet, t_B,
4. Angle of corrugations, θ,
5. Height of the sandwich panel (center-to-center distance between top and bottom face sheets), *h*,
6. Length of a unit-cell of the panel, 2*p*.
7. Number of unit-cell in the panel, *n*.

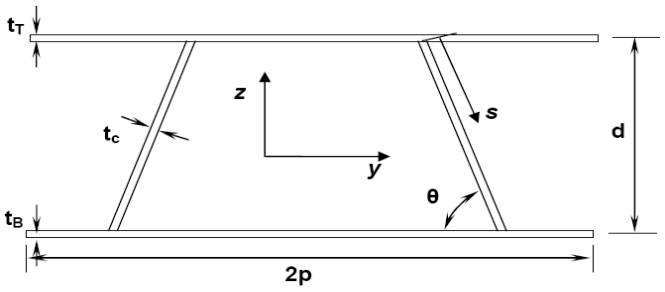

Figure 2. Unit-cell of the corrugated-core sandwich structure.

The *z*-axis is in the thickness direction of the ITPS panels. Parallel to the *y*-axis is the stiffer longitudinal direction, and the transverse direction is the *x* axis. The unit cell consists of two inclined webs and two thin face sheets. The unit cell is symmetric with respect to the *yz*-plane. Previous researchers adopted these assumptions in the derivation of stiffness parameters of sandwich panels with corrugated core (Libove and Hubka [6,7], C-core, Fung et. al. [13], and Z-core [14]). The top face sheet panel of the ITPS is required to withstand extreme reentry temperatures, have good impact resistance, high service temperatures, and high strength. The web acts as the heat conduction path from the top face sheet to the bottom face sheet. It also acts as a load bearing member by supporting most of the transverse shearing loads. To decrease the amount of heat that is conducted to the bottom face sheet, the web must either have a small thickness and low heat conductivity. Therefore material used for the top face sheet and web are titanium alloys (Ti-6Al-4V) because of their high stiffness and high service temperature. The bottom face sheet is expected to be a heat sink for the ITPS; therefore a material that has a high heat capacity is needed for the bottom face sheet. The bottom face sheet will also experience a major portion of the in-plane stresses because of the attachment mechanisms of stringers and frames to the space vehicle. Therefore, a high Young's Modulus material with a high heat capacity is suitable for the bottom face sheet. Therefore, the material used for the bottom face sheet is a beryllium alloy. The homogenization method also works well for other material combination including composite materials. The agreement is found to be good with the 3D ITPS panel analysis.

III. Unit Cell Analysis

Micromechanical finite element analysis of a unit cell was performed to determine the structure's extensional, bending, coupling and transverse shear stiffness of the equivalent orthotropic plate. This would require the prediction of the effective (macroscopic) properties of the panel from its constituent (microscopic) components - the top face sheet, bottom face sheets and the webs. The relationship between the unit cell macro stresses and macro strains provided the constitutive relations for the material [5]. Thus, the in-plane extensional and shear response and out-of-plane (transverse) shear response of an orthotropic panel are governed by the following constitutive relation:

$$\begin{bmatrix} N_x \\ N_y \\ Q_y \\ Q_x \\ N_{xy} \\ M_x \\ M_y \\ M_{xy} \end{bmatrix} = \begin{bmatrix} A_{11} & A_{12} & 0 & 0 & 0 & B_{11} & B_{12} & 0 \\ A_{12} & A_{22} & 0 & 0 & 0 & B_{12} & B_{22} & 0 \\ 0 & 0 & A_{44} & 0 & 0 & 0 & 0 & 0 \\ 0 & 0 & 0 & A_{55} & 0 & 0 & 0 & 0 \\ 0 & 0 & 0 & 0 & A_{66} & 0 & 0 & B_{66} \\ B_{11} & B_{12} & 0 & 0 & 0 & D_{11} & D_{12} & 0 \\ B_{12} & B_{22} & 0 & 0 & 0 & D_{12} & D_{22} & 0 \\ 0 & 0 & 0 & 0 & B_{66} & 0 & 0 & D_{66} \end{bmatrix} \begin{Bmatrix} \varepsilon_{x0} \\ \varepsilon_{y0} \\ \gamma_{yz} \\ \gamma_{xz} \\ \gamma_{xy0} \\ \kappa_x \\ \kappa_y \\ \kappa_{xy} \end{Bmatrix} \quad (1)$$

For considering the ITPS panel as an orthotropic plate, the following assumptions were made:

a) The displacements are small compared to the panel thickness.

b) The corrugated core has more bending stiffness along the *x*-axis than along the *y*-axis.
c) The ITPS panel has a much larger *L/d* ratio, say greater than eight, for the homogenization to be applicable.
d) The plate deformation in the thickness direction is negligible.
e) There is no local buckling on the face sheets and the core thickness remains constant.

Unlike the analytical models presented in [11], the face sheets and web laminates need not be symmetric with respect to their own mid-planes and also the top and bottom face sheets need not be identical as the FE approach can capture any variable material properties and geometries.

An FE analysis is performed on the unit cell using the commercial ABAQUS® finite element program. The ITPS unit cell is modeled with eight node shell elements and the stiffness properties are obtained by forcing the unit cell to six linearly independent deformations. Deformations, in-plane strains, and curvatures are imposed on the FEM model by enforcing periodic displacement boundary conditions derived in the next section. To prevent rigid body motion one of the corner nodes is also fixed.

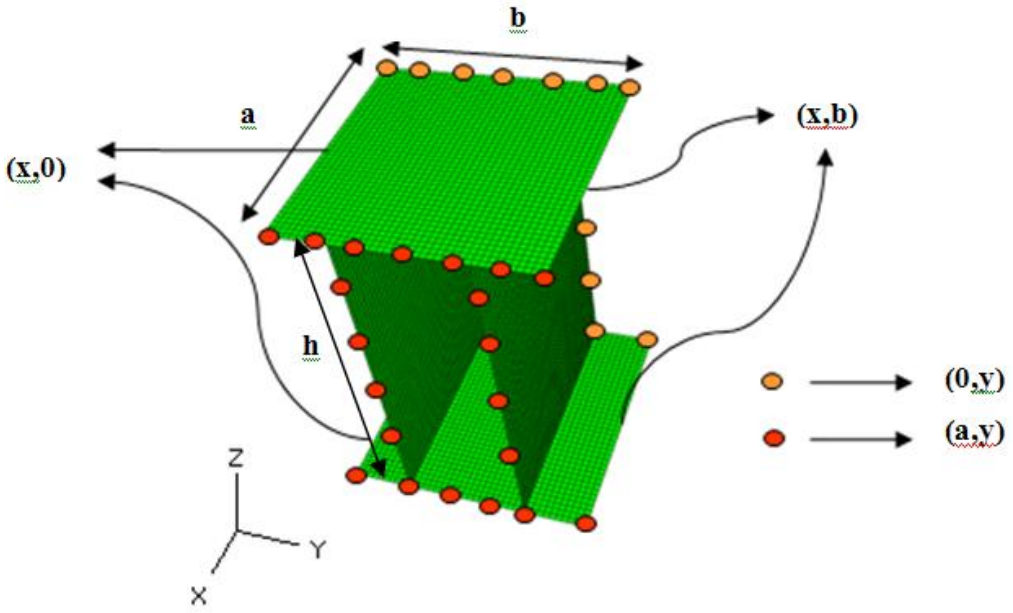

Figure 3. Finite element model of the unit cell.

The following assumptions are made in the derivation of the periodic boundary conditions:

a) Materials are homogeneous and orthotropic in macro scale.
b) Plate is assumed to be in the xy-plane with unit cells repeating in the x and y directions.
c) The plate is subjected to a uniform state of strain in the macroscopic sense.
d) All unit cells have identical stress and strain fields in micro scale. For the continuity of micro stresses across the unit cell it is required that tractions are equal and opposite at corresponding points on opposite faces of the unit cell.

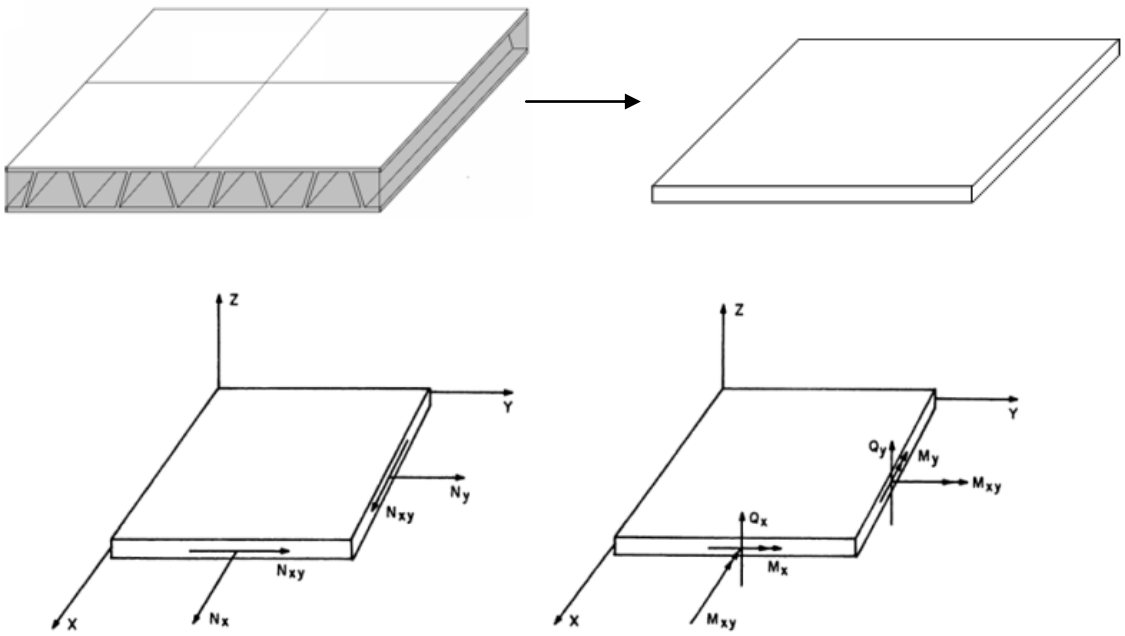

Figure 4. ITPS panel is modeled as thick, orthotropic plate. For obtaining the ABD Stiffness, it is subjected to uniform state of strain in macroscopic sense and hence subjected to uniform force and moment resultant [15].

A. Periodic Boundary Conditions

For the derivation of periodic boundary condition, we will consider the displacement field $u(x, y, z), v(x, y, z)$ and $w(x, y, z)$ within the unit cell, which is a hexahedron of size $a \times b \times h$. Our goal is to determine a set of boundary conditions that need to be applied on the surfaces of the unit cell such that the average strain in the unit cell is equal to a given value. There are infinite sets of BCs for a given average strain. However, when the condition of periodicity is imposed, the periodic BCs become almost unique. In the following we derive the periodic BCs for various average deformations.

If the unit cell deforms like a plate, then it will have an average strain and curvature which will be equal to the corresponding mid-plane strain and curvature. We will start our derivation by considering the case for average strain $\bar{\varepsilon}_x$.

1. Average strain = $\bar{\varepsilon}_x$

The volume average of the strain is expressed as

$$\bar{\varepsilon}_x = \frac{1}{V}\int_V \frac{\partial u}{\partial x} dV \tag{2}$$

Applying divergence theorem we obtain the surface integral

$$\bar{\varepsilon}_x = \frac{1}{V}\int_S u n_x dS \tag{3}$$

where, S is the surface of the unit cell. Since $n_x = 0$ on all surfaces except the two surfaces normal to the x-axis, the above integral can be written as

$$\bar{\varepsilon}_x = \frac{1}{V}\int_{S_x}\big(u(a,y,z)-u(0,y,z)\big)\,dS_x = \frac{1}{V}\int_{-h/2}^{+h/2}\int_{0}^{b}\big(u(a,y,z)-u(0,y,z)\big)\,dydz \tag{4}$$

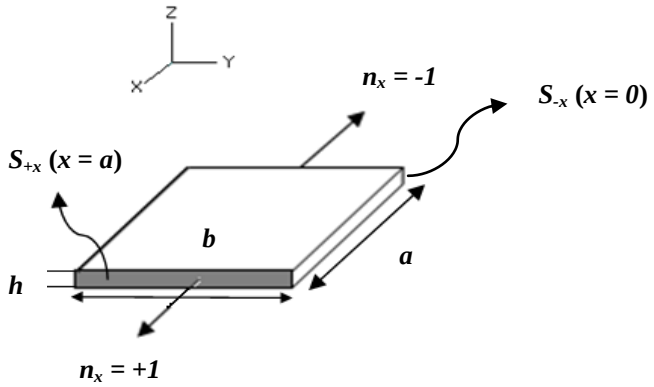

Figure 5. n_x is the outward unit normal, which has a value of +1 and -1 as shown and is equal to zero in the remaining faces.

At this point it is worth noting that the various unit cells must undergo identical deformations for obtaining the equivalent ABD stiffness property. This requires that the deformed surface S_{+x} (x=a) should be obtained by translating and rotating the deformed surface S_{-x} (x=0) Then one can write

$$\begin{aligned} u(a,y,z)-u(0,y,z) &= C_1 + R_1 z \\ v(a,y,z)-v(0,y,z) &= C_2 \\ w(a,y,z)-w(0,y,z) &= C_3 + R_2 y \end{aligned} \tag{5}$$

where, C_1, C_2 and C_3 represent the rigid body translation in the x, y and z directions, respectively, and R_1 and R_2 represent magnitudes of rotations about the y- and x-axis, respectively. Similarly one can write the relative displacements between the surfaces S_{+y} (y=b) and S_{-y} (y=0):

$$\begin{aligned} u(x,b,z)-u(x,0,z) &= C_4 \\ v(x,b,z)-v(x,0,z) &= C_5 + R_3 z \\ w(x,b,z)-w(x,0,z) &= C_6 + R_4 x \end{aligned} \tag{6}$$

Substituting the first equation in Eq. (5) in Eq. (4) we obtain

$$\bar{\varepsilon}_x = \frac{1}{V}\int_{-h/2}^{+h/2}\int_{0}^{b}\big(C_1 + R_1 z\big)\,dydz = \frac{C_1 bh}{abh} = \frac{C_1}{a} \Rightarrow \boxed{C_1 = a\bar{\varepsilon}_x} \tag{7}$$

We infer the constant C_1 is equal to $a\bar{\varepsilon}_x$.

2. Average curvature = $\bar{\kappa}_x$

The average rotation at a point (x,y) in the unit cell can be defined as

$$\bar{\psi}_x(x,y) = \frac{1}{h}\int_{-h/2}^{+h/2} \frac{1}{2z}\big(u(x,y,+z) - u(x,y,-z)\big)dz \tag{8}$$

Then the average curvature can be derived as

$$\bar{\kappa}_x = \frac{1}{abh}\int_0^b\int_0^a \frac{\partial \bar{\psi}_x}{\partial x}\,dxdy = \frac{1}{abh}\int_0^b\int_0^a\int_{-h/2}^{+h/2} \frac{1}{2z}\left(\frac{\partial u(x,y,+z)}{\partial x} - \frac{\partial u(x,y,-z)}{\partial x}\right)dzdxdy \tag{9}$$

Applying divergence theorem as before and following the procedures used to derive Eq. (7) we obtain

$$\bar{\kappa}_x = \frac{1}{abh}\int_{-h/2}^{+h/2}\int_0^b \frac{1}{2z}\Big[\big(u(a,y,z) - u(0,y,z)\big) - \big(u(a,y,-z) - u(0,y,-z)\big)\Big]dydz \tag{10}$$

Substitution of the first of Eq. (5) into the above equation yields

$$\begin{aligned}\bar{\kappa}_x &= \frac{1}{abh}\int_{-h/2}^{+h/2}\int_0^b \frac{1}{2z}\Big[\big(C_1 + R_1 z\big) - \big(C_1 - R_1 z\big)\Big]dydz \\ &= \frac{R_1}{a} \Rightarrow \boxed{R_1 = a\bar{\kappa}_x}\end{aligned} \tag{11}$$

3. Average transverse shear strain = $\bar{\gamma}_{xz}$

The transverse shear strain in the plate context is defined as $\bar{\gamma}_{xz} = \psi_x + \dfrac{\partial w}{\partial x}$. We will use this relation to derive BCs for the *w* displacement. The average transverse shear strain is defined as

$$\begin{aligned}\bar{\gamma}_{xz} &= \frac{1}{abh}\int_{-h/2}^{+h/2}\int_0^b\int_0^a \gamma_{xz}\,dxdydz \\ &= \frac{1}{abh}\int_{-h/2}^{+h/2}\int_0^b\int_0^a \left(\psi_x + \frac{\partial w}{\partial x}\right)dxdydz \\ &= \frac{1}{abh}\int_{-h/2}^{+h/2}\int_0^b\int_0^a \psi_x\,dxdydz + \frac{1}{abh}\int_0^c\int_0^b\int_0^a \frac{\partial w}{\partial x}\,dxdydz\end{aligned} \tag{12}$$

By using the procedures in Section III.A.1 (*Average strain* = $\bar{\varepsilon}_x$) and Section III.A.2 (*Average curvature* = $\bar{\kappa}_x$) above, the second term on the RHS of the above equation can be easily converted into boundary conditions on *w*. However, since the first term on the RHS does not have any derivative therefore cannot be converted into a boundary integral we will use the best available approximation for ψ_x. The definition of average curvature $\bar{\kappa}_x$ can be used to obtain an approximation for ψ_x as $\psi_x = \psi_x(0) + \bar{\kappa}_x x$. Substituting in Eq. (12) we obtain,

$$\bar{\gamma}_{xz} = \bar{\kappa}_x \frac{a}{2} + \frac{1}{V}\int_{-h/2}^{+h/2}\int_0^b \big(w(a,y,z) - w(0,y,z)\big)\,dydz \tag{13}$$

The *w* displacements in the above integral must satisfy the periodicity condition in Eq. (5). Substituting $w(a,y,z) - w(0,y,z) = C_3 + R_2 y$ we obtain

$$\bar{\gamma}_{xz} = \bar{\kappa}_x \frac{a}{2} + \frac{C_3}{a} \tag{14}$$

Then, the constant C_3 is obtained as

$$\boxed{C_3 = a\bar{\gamma}_{xz} - \bar{\kappa}_x \frac{a^2}{2}} \tag{15}$$

Using similar procedures one can derive the other constants in Eq. (5) and Eq. (6) as,

$$\begin{aligned} C_2 &= a\overline{\left(\frac{\partial v}{\partial x}\right)},\ C_4 = a\overline{\left(\frac{\partial u}{\partial y}\right)},\ C_5 = b\bar{\varepsilon}_y \\ C_6 &= \left(b\bar{\gamma}_{yz} - \frac{b^2}{2}\bar{\kappa}_y\right),\ R_3 = b\bar{\kappa}_y \\ R_2 &= a\overline{\left(\frac{\partial^2 w}{\partial x \partial y}\right)},\ R_4 = b\overline{\left(\frac{\partial^2 w}{\partial x \partial y}\right)} \end{aligned} \tag{16}$$

where an over bar indicates average quantity. Thus the eight constants in the periodic BCs of Eq. (5) and Eq. (6) are given in terms of the average mid-plane strains and curvatures of the plate. The periodic BCs are summarized in the following table for unit values of the mid-plane strains and curvatures. We have assumed that the transverse shear strains are equal to zero for the BCs in Table 1.

Table 1. The *u*, *v*, and *w* sets of periodic boundary conditions for the solid elements. Superscript M stands for macro scale deformations.

	u(a,y) – u(0,y)	***v(a,y) – v(0,y)***	***w(a,y) – w(0,y)***	***u(x,b) – u(x,0)***	***v(x,b) – v(x,0)***	***w(x,b) – w(x,0)***
$\varepsilon_{x0}^{M} = 1$	*a*	*0*	*0*	*0*	*0*	*0*
$\varepsilon_{y0}^{M} = 1$	*0*	*0*	*0*	*0*	*b*	*0*
$\gamma_{xy0}^{M} = 1$	*0*	*a*/2	*0*	*b*/2	*0*	*0*
$\kappa_x^{M} = 1$	*az*	*0*	$-a^2/2$	*0*	*0*	*0*
$\kappa_y^{M} = 1$	*0*	*0*	*0*	*0*	*bz*	$-b^2/2$
$\kappa_{xy}^{M} = 1$	*0*	*az*/2	*-ay*/2	*bz*/2	*0*	*-bx*/2

The above BCs are in terms of the *u*, *v* and *w* displacements, and are adequate if one uses solid elements. However, if structural elements, e.g., plate elements, are used to model the unit-cell, then the above BCs have to be modified to impose BCs on rotations θ_x and θ_y. The modified BCs are presented below:

Table 2. The six sets of periodic boundary conditions applied to the unit cell to determine the *A*, *B* and *D* matrices of the equivalent orthotropic plate. Superscript M stands for macro scale deformations.

	$u(a,y) - u(0,y)$	$v(a,y) - v(0,y)$	$w(a,y) - w(0,y)$	$u(x,b) - u(x,0)$	$v(x,b) - v(x,0)$	$w(x,b) - w(x,0)$	$\theta_x(a,y) - \theta_x(0,y)$	$\theta_y(a,y) - \theta_y(0,y)$	$\theta_x(x,b) - \theta_x(x,0)$	$\theta_y(x,b) - \theta_y(x,0)$
$\varepsilon_{x0}^{M} = 1$	a	0	0	0	0	0	0	0	0	0
$\varepsilon_{y0}^{M} = 1$	0	0	0	0	b	0	0	0	0	0
$\gamma_{xy0}^{M} = 1$	0	$a/2$	0	$b/2$	0	0	0	0	0	0
$\kappa_{x}^{M} = 1$	az	0	$-a^2/2$	0	0	0	a	0	0	0
$\kappa_{y}^{M} = 1$	0	0	0	0	bz	$-b^2/2$	0	0	$-b$	0
$\kappa_{xy}^{M} = 1$	0	$az/2$	$-ay/2$	$bz/2$	0	$-bx/2$	$-a/2$	0	0	$b/2$

The nodal stresses of the boundary nodes are obtained from the finite element output and nodal moments are obtained by multiplying the nodal forces by the distance from the mid plane. The nodal forces and moments of the boundary nodes are then summed to obtain the force and moment resultants as

$$\begin{aligned} \left[N_i, M_i\right] &= \frac{1}{b}\sum_m \left[1, z\right] F_i^{(m)}(a, y, z) \;\rightarrow\; \text{For the face } x = a \\ \left[N_i, M_i\right] &= \frac{1}{a}\sum_m \left[1, z\right] F_i^{(m)}(x, b, z) \;\rightarrow\; \text{For the face } y = b \end{aligned} \tag{17}$$

The values obtained from the above equations give the stiffness coefficients in the column corresponding to the non zero deformations in Eq. (1) and thus applying the six independent deformations we can populate the stiffness matrix in Eq. (1).

IV. Transverse Shear Stiffness A_{44} and A_{55}

Past studies have indicated that the corrugated core sandwich panels have low transverse shear rigidity and thus transverse shear deformations are significant. Therefore, there is a need to estimate the transverse shear stiffness terms A_{44} and A_{55} for the equivalent orthotropic plate. Below we describe a finite element based method to obtain the required transverse shear stiffness properties, A_{44} and A_{55}.

In the present approach we consider a beam that consists of one unit cell in the width direction and about ten unit cells in the length direction. The beam is clamped at one end. The beam is subjected to either a transverse load at the tip or a uniformly distributed load. The deflection of the plate is obtained using a one dimensional plate with unit cells in one direction (x and y direction for A_{55} and A_{44}, respectively). The transverse deflection obtained is compared with the classical plate theory deflection, which consists of bending and shears deflections in order to estimate the transverse shear stiffness.

A. Cantilever Beam under Transverse Load

We will illustrate this method by deriving A_{55}. The same method can be use for finding A_{44} as well. We will consider a one-dimensional plate with 20 unit cells along the x axis. (Fig. 6) with fixed displacement and rotations on the face $(0,y)$. We constrained the deformations along the faces $(x,0)$ and $(x,2p)$ and apply equal vertical displacement to all the nodes on the face ($x = L_{ex} = a$) . Then, on the face ($x = L_{ex} = a$), we apply a transverse shear force, $Q_x = 1$ on the TFS and obtain the maximum deflection at the tip from the analysis (Fig. 6).

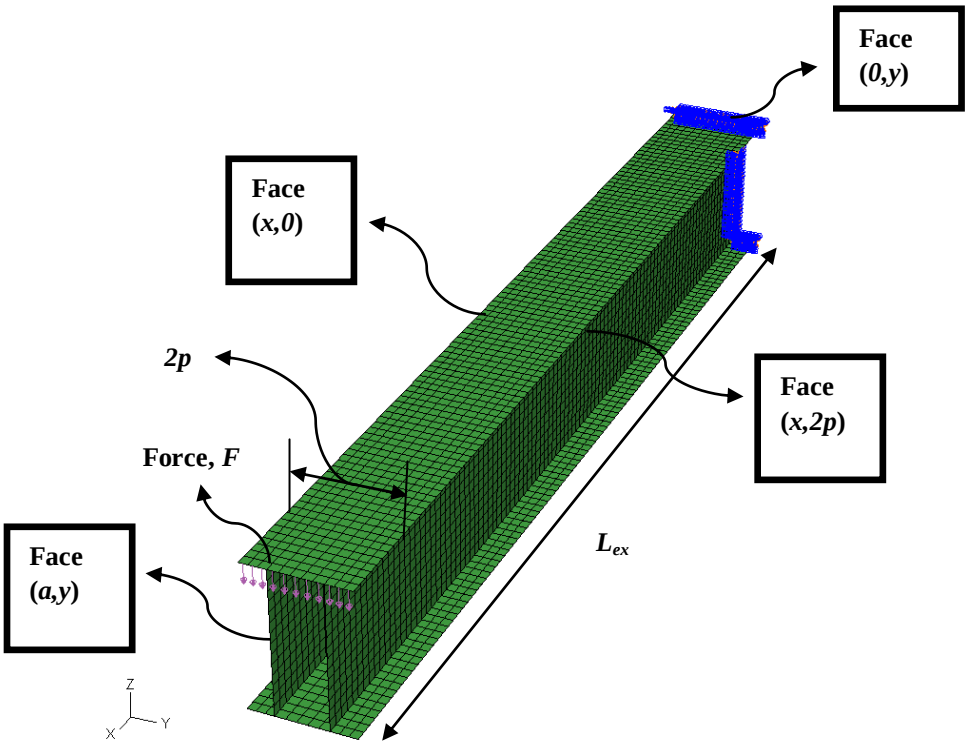

Figure 6. Typical mesh and finite element model for the estimation of transverse shear stiffness A_{55}, when subjected to transverse shear force Q_x.

Using shear deformable plate theory [15] one can derive an expression for the transverse deflection as:

$$w(L_{ex}) = -\frac{FL_{ex}}{2pA_{55}} - \frac{FL_{ex}^{3}}{2p}\frac{1}{3D_{11}^{'}}$$
$$D_{11}^{'} = D_{11} - \frac{B_{11}^{2}}{A_{11}} \tag{18}$$

From the total deflection, $w(L_{ex})$, which is composed of shear and bending deflection, and since we know $D_{11}^{'}$ we can calculate the stiffness A_{55} from Eq. (18).

Using a similar method we can derive the transverse shear stiffness (A_{44}). Again, the total deflection, w is composed of shear and bending deflection, as given by Eq.(19).

$$w(L_{ey}) = -\frac{FL_{ey}}{2pA_{44}} - \frac{FL_{ey}^{3}}{2p}\frac{1}{3D_{22}^{'}}$$
$$D_{22}^{'} = D_{22} - \frac{B_{22}^{2}}{A_{22}} \tag{19}$$

B. Cantilever Beam, with Pressure Load on the Top Face Sheet

We can also find the transverse shear stiffness properties A_{44} and A_{55}, by applying a pressure load on to the top face sheet of the one-dimensional plate (Fig. 7). Again, using shear deformable plate theory [15] one can derive an expression for the end transverse deflection as:

$$w(L_{ey}) = -\frac{P_0 L_{ey}^2}{2A_{44}} - \frac{P_0 L_{ey}^4}{8D_{22}^{'}}$$
$$D_{22}^{'} = D_{22} - \frac{B_{22}^2}{A_{22}} \tag{20}$$

From the total deflection, $w(L_{ey})$ which is composed of shear and bending deflection, we calculate the stiffness A_{44}, as given by the Eq. (20). Similarly, we can also derive for A_{55} as well.

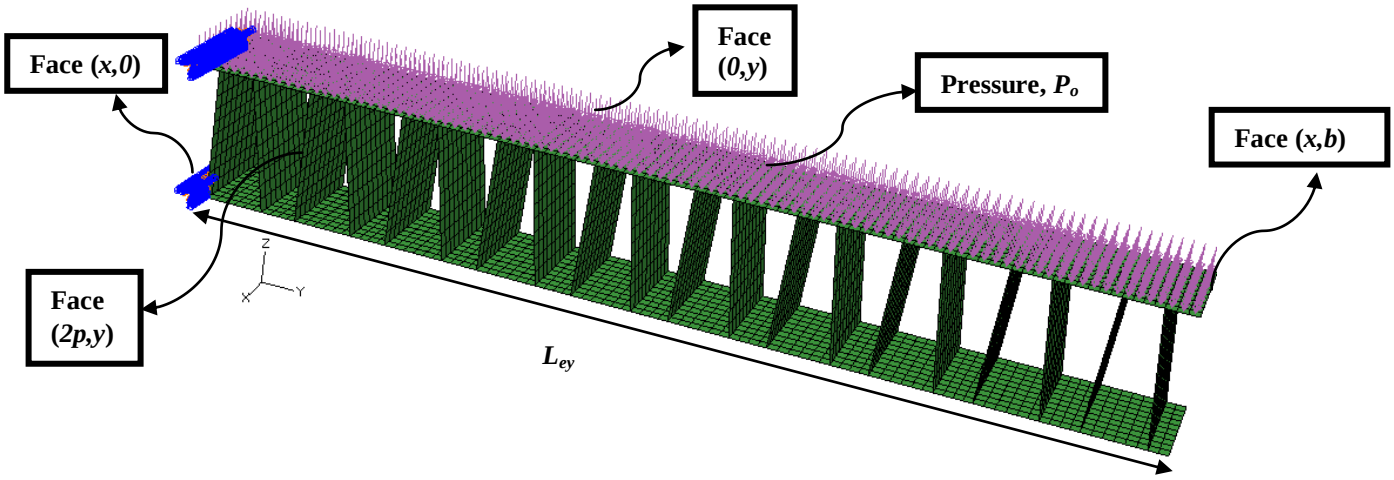

Figure 7. Typical mesh and finite element model for the estimation of transverse shear stiffness A_{44}.

C. Simply Supported Beam, with Pressure Load on the Top Face Sheet

The procedures described for a cantilevered plate beam can be repeated for simply supported beam. The free body diagram for the simply supported plate is given in Fig. 8.

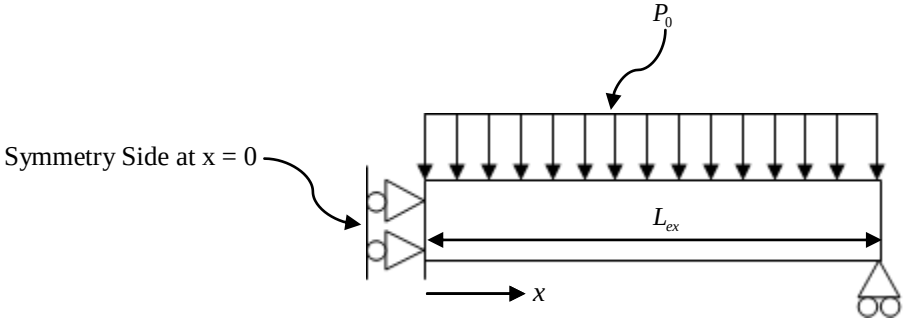

(Free Body Diagram)

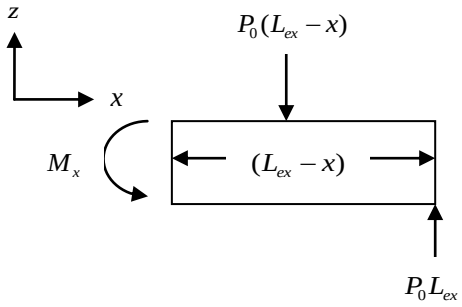

Figure 8. Simply supported beam with pressure P_0 and the free body diagram used for the derivation.

From the total end deflection, *w(0)* which is composed of shear and bending deflection, we calculate the stiffness A_{55}, as given by the Eq.(21). Similarly, we can derive A_{44} as well.

$$w(0) = -\frac{5P_0 L_{ex}^{\ 4}}{24D_{11}^{'}} - \frac{P_0 L_{ex}^{\ 2}}{2A_{55}}$$
$$D_{11}^{'} = D_{11} - \frac{B_{11}^2}{A_{11}} \tag{21}$$

The *ABD* matrices and the transverse shear stiffness A_{44} and A_{55} obtained using homogenization are then inputted into the FE program for the two-dimensional homogenized plate analysis. We will validate our calculation of the transverse shear stiffness by assuming it as a shear deformable plate and compare the maximum transverse deflection with the 3D model under the pressure load as discussed in Section V.

V. Results

For verification of the effectiveness of the FE based homogenization method, consider a corrugated-core sandwich panel unit cell with the following dimension: p = 25 mm, d = 70 mm, t_{TF} = 1.2 mm, t_{BF} = 7.49 mm, t_w = 1.63 mm, $\theta = 85^o$. For the 3D FE analysis we assume that the whole panel consists of 40 unit cells. In the example, the TFS and the web are modeled using Titanium alloy Ti-6Al-4V (E_1 = 109.36 GPa and v = 0.3) and the BFS is modeled using Beryllium alloy (E_1 = 290.482 GPa and v = 0.063). For the 3D FE model, one fourth of the ITPS panel containing half the total number of unit cells is modeled using ABAQUS® finite element (FE) software. The model uses approximately 75,000 eight-node shell elements (S8R). The mesh convergence was ascertained by reducing the dimension of the element's edges by half and repeatedly solving the pressure analysis till the maximum transverse deflection was less than 2%. The boundary conditions considered are: fixed vertical displacements for the bottom face sheet (BFS) and fixed rotations for the top face sheet (TFS) on the edges of the panel. On the symmetricedges, symmetric boundary conditions are used.

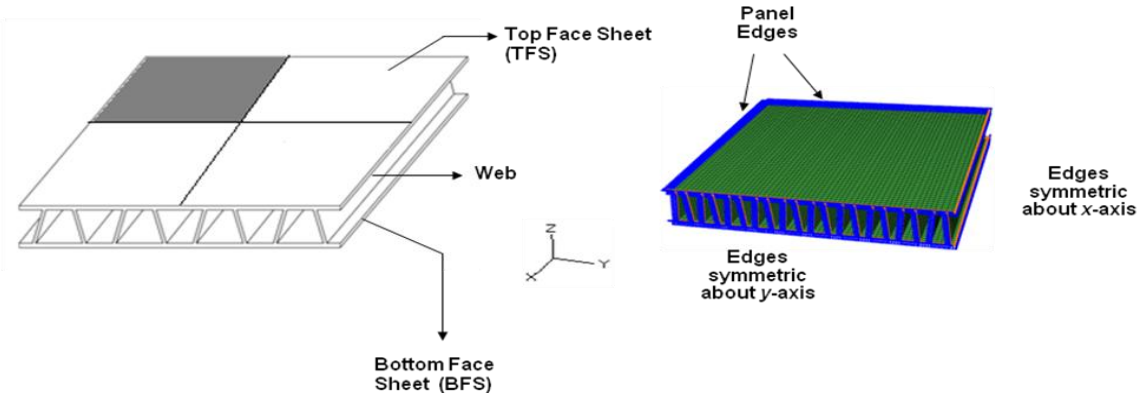

a) **b)**

Figure 9. a) The ITPS Panel b) Typical mesh and boundary conditions for the 3D finite element model of one fourth of the panel

For the homogenized model, again the one-fourth plate is used due to symmetry. Shell elements in ABAQUS® finite element (FE) software were used. The model used a total of 40,400 eight-node shell elements (S8R). A simply supported boundary condition is considered along the boundary of the plate. The plate edges are allowed to move in the horizontal plane.

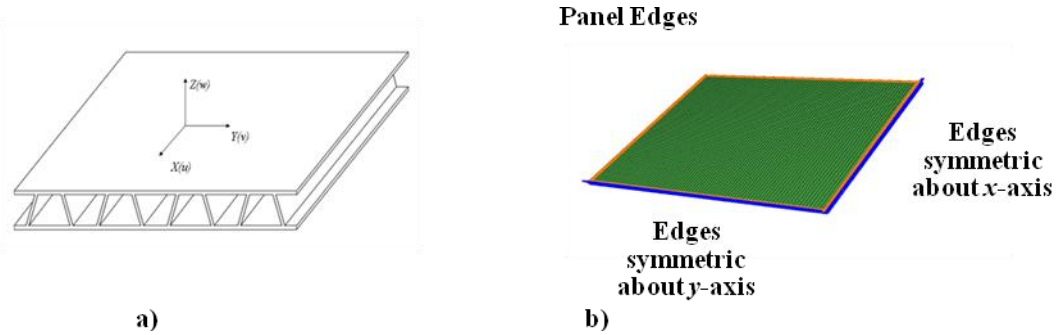

a) **b)**

Figure 10. a) One fourth of the ITPS panel, b) Typical mesh and boundary conditions for the low fidelity 2D finite element model

The equivalent stiffness constants of the orthotropic plate are obtained by forcing the unit cell to six linearly independent deformations as mentioned before. The results are given below:

$$[A]=\begin{bmatrix} 2.83 & 0.18 & 0 \\ 0.18 & 2.33 & 0 \\ 0 & 0 & 1.07 \end{bmatrix}\times 10^{9}\,\frac{N}{m},\quad [B]=\begin{bmatrix} -71.45 & -3.36 & 0 \\ -3.36 & -71.45 & 0 \\ 0 & 0 & -34.05 \end{bmatrix}\times 10^{6}\,N$$

$$[D]=\begin{bmatrix} 3.06 & 0.22 & 0 \\ 0.22 & 2.85 & 0 \\ 0 & 0 & 1.32 \end{bmatrix}\times 10^{6}\,N-m$$

Due to different thicknesses and different material properties of the TFS and BFS, there will be a coupling between the extensional and bending deformations.

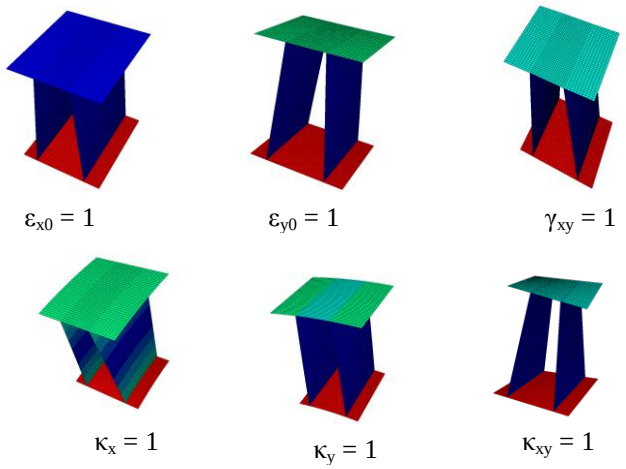

Figure 11. Unit cell deformations when periodic boundary conditions are imposed.

A. Prediction of Transverse Shear Stiffness using different Boundary Conditions

As mentioned in Section IV, we have predicted the transverse shear stiffnesses, A_{44} and A_{55} by applying transverse shear force and the pressure load for different boundary conditions. We have considered a corrugated-core sandwich panel unit cell with the dimension mentioned above. Here, we will only show the estimation of A_{44} using different boundary conditions. We obtain a similar value using any of the boundary conditions as seen in Fig. 12.

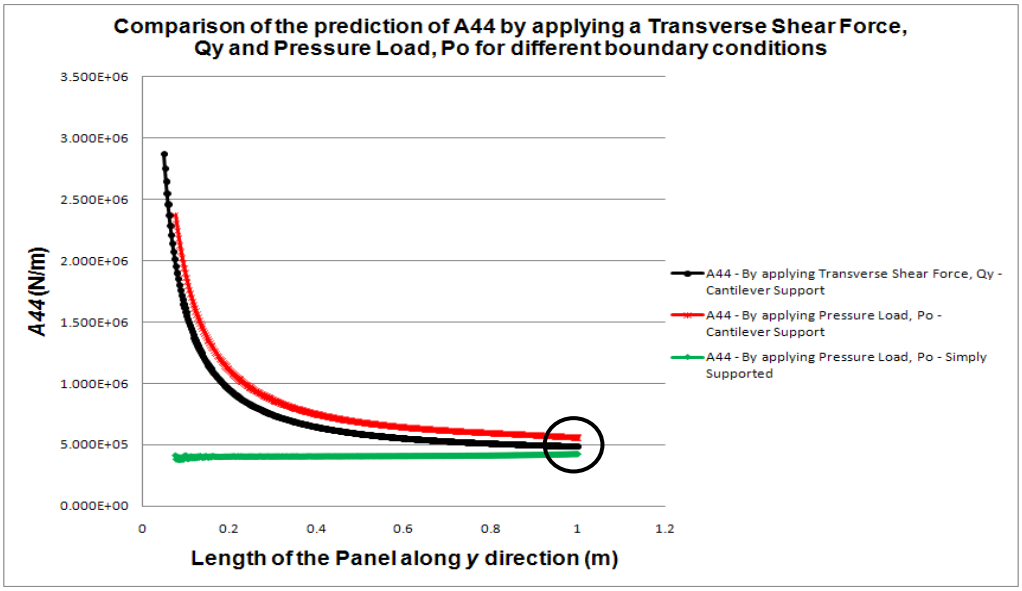

Figure 12. Prediction of transverse shear stiffness A_{44}, under various boundary conditions and loading conditions.

Initially, we started with a one dimensional beam analysis for 6 unit cells. For that case, the boundary condition for the cantilever beam at the end provides some inaccuracies which is not the case for the ideal beam solution. The boundary condition for the simply supported beam was more relaxed and hence it converges very fast. Therefore we increase the number of unit cells to 20 until all of the three boundary conditions yield similar results. This value of

transverse shear stiffness is also verified by comparing the maximum transverse deflection under pressure load with the 3D model.

B. Variation of the ABD Stiffness and the Transverse Shear Stiffness with the change in web inclination

Past studies [16] have indicated that the behavior of the stiffness of the corrugated core sandwich panels varies with the web angle inclination. Changes in A_{44} and A_{55} are important as it contributes to the panel deflection under pressure loading case. Consider the truss core sandwich panel of the following dimension: p = 84.25 mm, d = 70 mm, t_{TF} = 1.2 mm, t_{BF} = 7.49 mm, t_w = 1.63 mm, a = 1.6845 m, b = 1.6845 m. The material used for the TFS and web is Titanium alloy and Beryllium alloy for the BFS. The thickness of the web is described in such a way that the cross sectional area or the weight remains same for any given web angle. By doing this we can understand the behavior of the stiffness to the change in angle only rather than changing the angle and area. Below are the results obtained.

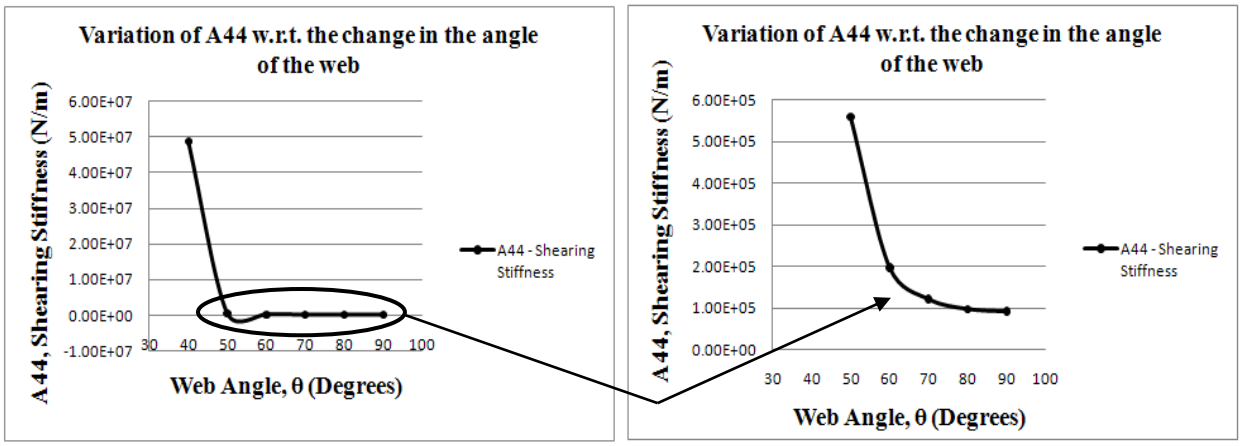

Figure 13. Variation for the transverse shear stiffness A_{44} with web angle. The transverse shear stiffness A_{44} is calculated by subjecting the plate to a uniformly distributed load for a cantilever support.

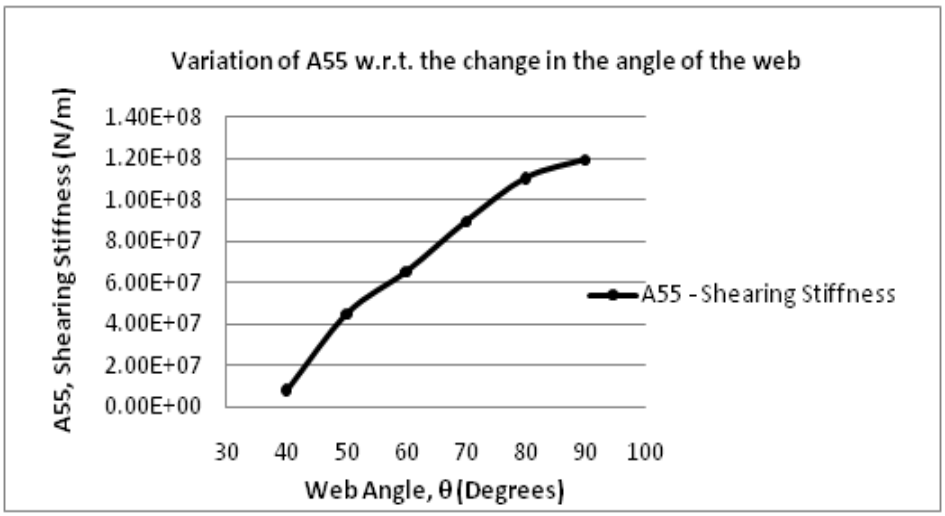

Figure 14. Variation for the transverse shear stiffness, A_{55} with the change in the angle of the web. The transverse shear stiffness A_{44} is calculated by subjecting the plate to a uniformly distributed load for a cantilever support.

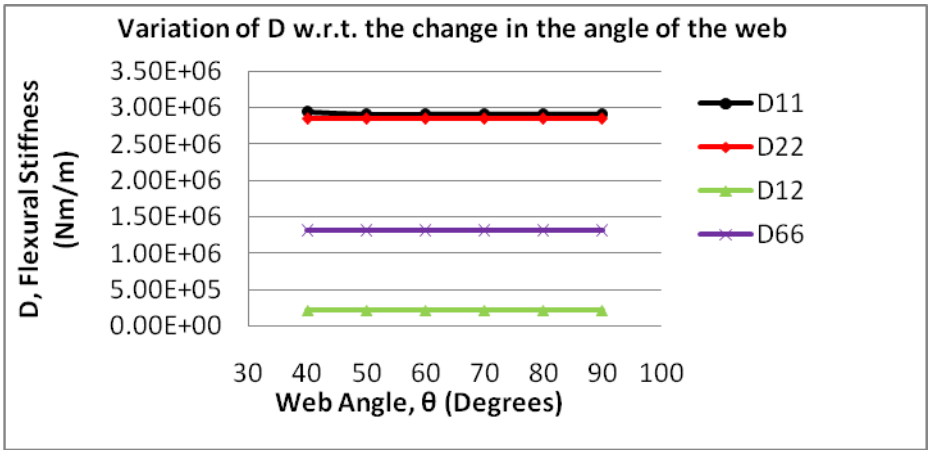

Figure 15. Variation for the flexural stiffness, *D* with the change in the angle of the web.

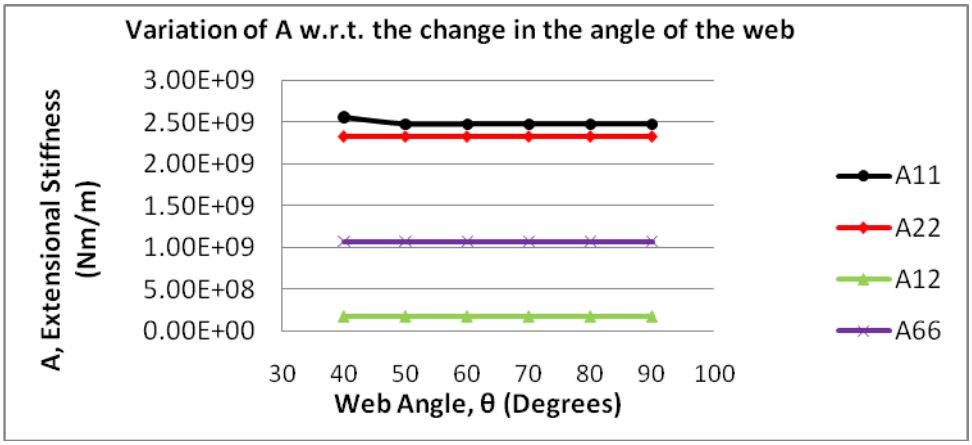

Figure 16. Variation for the extensional stiffness, *A* with the change in the angle of the web.

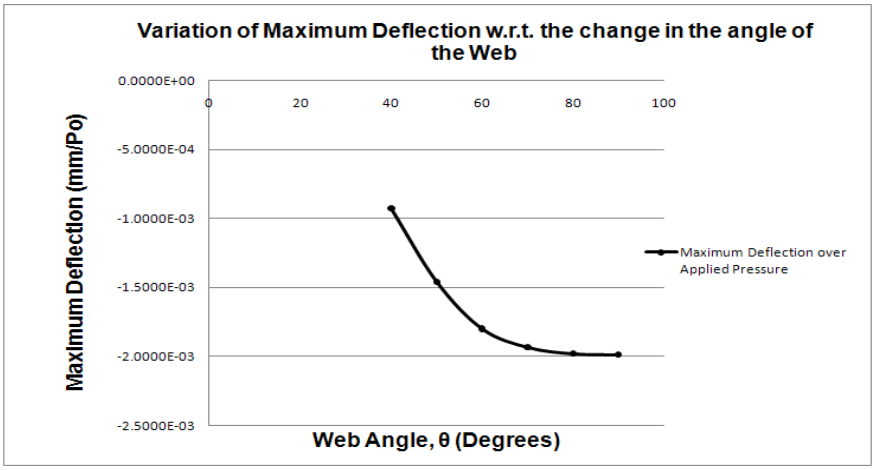

Figure 17. Variation for the maximum deflection, *w* under the applied pressure with the change in the angle of the web.

Some of the conclusions obtained from the above figure are also in agreement with the paper [16] and are as follows:

a) The triangular webs have the maximum A_{44} shear stiffness for the truss-core sandwich panels. Triangular webs have the maximum length of the web for a given d and hence it has the maximum A_{44} shear stiffness.
b) The variation in the transverse shear A_{55} with change in web inclination is not as much as A_{44}, but the maximum value of A_{55} is when the web angle is 90^o.

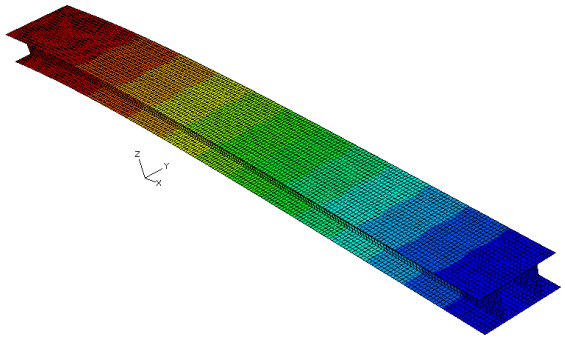

Figure 18. Truss-core sandwich panels with web angle as 90^o have the maximum transverse shear stiffness A_{55}.

c) The extensional stiffness, A11 and the bending stiffness, D11 and the transverse shear stiffness A44 decreases with the web angle while the transverse shear stiffness A55 increases. The other extensional and bending stiffness remains almost constant (Fig. 15 and Fig. 16).
d) Maximum deflection occurs at rectangular web angle, and minimum deflection occurred at the triangular web configuration.

D. Validation of the ABD Stiffness and the Transverse Shear Stiffness

The extension, bending, coupling and the transverse shear stiffnesses calculated above are validated by assuming the corrugated core sandwich panel of the ITPS as a thick plate that is continuous, orthotropic, and homogeneous. We apply the transverse pressure of 101 kPa on to the plate model and compare the maximum deflection in the z direction for the 2D model with the 3D model. A simply supported boundary condition is considered along the boundary of the plate. The plate edges are allowed to move in the horizontal plane. Due to symmetry only one-fourth of the panel is modeled. Initially, we used the classical laminate plate theory (Kirchhoff plate) in which we only input the *ABD* matrices and assume the transverse shear stiffness to be infinitely large. Then, we considered the transverse shear stiffness properties, A_{44} and A_{55}, and performed the analysis using shear-deformable elements (shear deformable plate theory).

For the 3D ITPS model, again the pressure load of 101 kPa is applied on the TFS. The boundary conditions considered are used as mentioned before. For the 3D ITPS panel, we compare the maximum deflection in the z direction for the TFS where the load is applied.

The maximum deflection was at the center. When we use the classical laminate plate theory (Kirchhoff plate), the percentage difference from the 3D model was 55% as compared using shear-deformable elements where the difference was only 3.6%. The results are shown in Table 3 and thus it validates that our calculation of the various stiffnesses are correct.

The material properties and the dimensions are used as before. The dimensions are: p = 25 mm, d = 70 mm, t_{TF} = 1.2 mm, t_{BF} = 7.49 mm, t_w = 1.63 mm, θ = 85^o and n = 20 unit cells in the whole panel.

Table 3. Effect of shear deformation on the maximum deflection at the center; comparison between the 3D analysis of the ITPS panel and 2D plate analyses.

Type of Analysis	w_{max} (m)	Percentage difference (%)
3D Analysis	1.194×10^{-3}	-
Classical plate theory	5.357×10^{-4}	55
Shear-deformable plate theory	1.151×10^{-3}	3.6

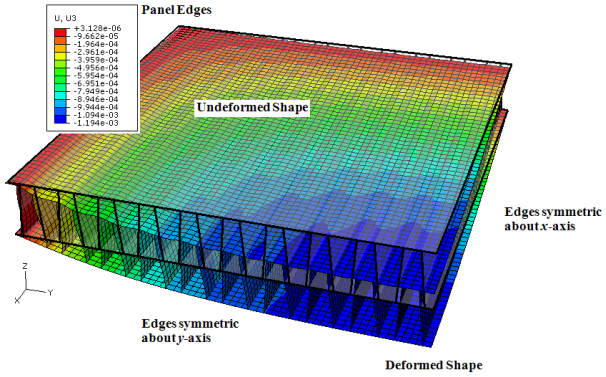

Figure 19. Undeformed and Deformed shape of the 3D ITPS panel, when subjected to transverse pressure of 101 kPa

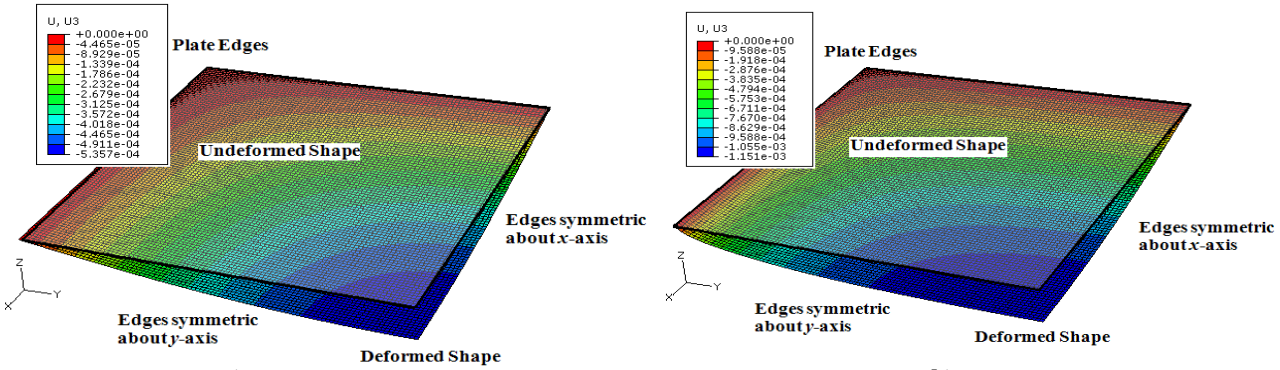

Figure 20. Undeformed and Deformed shape of the 2D plate model, when subjected to transverse pressure of 101 kPa. (a) Modeled using classical laminate plate theory (Kirchoff plate) by assuming the transverse shear stiffness to be infinitely large (b) Modeled using shear-deformable elements by considering the transverse shear stiffness properties.

VI. Summary

In this paper, a finite element based homogenization procedure is developed for modeling corrugate sandwich panels as 2D orthotropic plates. A detailed derivation of the periodic boundary condition is presented, which is used to obtain the bending, extensional, coupling, and shear stiffness for an ITPS panel from a finite element model. Also the derivation of the transverse shear stiffness properties are derived using FE approach and a comparison is made for various boundary condition and under different loading conditions. The finite element based micromechanical analysis is capable of handling any unsymmetrical material properties and thickness.

A sensitivity study for the various stiffness properties has also been done with the change in the angle of the web. Maximum deflection occurs for rectangular webs where as minimum deflection occurred at the triangular web configuration. For triangular webs, A_{44} has the maximum shear stiffness for the truss-core sandwich panels. Thus, the panels having triangular webs have negligible shear deformation, but it leads to other problems. Triangular webs tend to be longer in length and it could result in local buckling of the panels. The increased length will lead to a lower critical buckling value.

Predictions of various stiffnesses are also validated by applying a transverse pressure of 101 kPa on the 2D plate model and 3D ITPS panel and found the maximum deflection to be approximately equal.

Acknowledgements

This research is sponsored by NASA under a cooperative agreement (No. NNX08AB40A). Partial support was provided by a grant under the Constellation University Institutes Project (CUIP). Any opinions, findings, and conclusions or recommendations expressed in this material are those of the author(s) and do not necessarily reflect the views of the National Aeronautics and Space Administration.

References

[1]Blosser, M. L., "Advanced Metallic Thermal Protection Systems for Reusable Launch Vehicles," Ph.D. Dissertation, Mechanical and Aerospace Dept., University of Virginia, Charlottesville, VA, 2000.

[2]Blosser, M. L., "Development of Metallic Thermal Protection Systems for the Reusable Launch Vehicle", NASA TM-110296, Oct 1996.

[3]Behrens, B., Muller, M., "Technologies for Thermal Protection Systems applied on re-usable launcher," *Acta Astronautica*, Vol. 55, No. 3-9, Aug-Nov 2004, pp. 529-536.

[4]Chang, W., Venstel, E., Krauthammer, T., & John, J. (2005). Bending behavior of corrugated-core sandwich plates. Composite Structures, 70(1), 81-89.

[5]B.V. Sankar and R.V. Marrey (1993) "A Unit Cell Model of Textile Composite Beams for Predicting Stiffness Properties", Composites Science and Technology, 49(1):61-69.

[6]Libove, C., Hubka, R. E., "Elastic Constants for Corrugated Core Sandwich Plates," National Advisory Committee for Aeronautics Technical Note (NACA TN)-2289, 1951.

[7]Lok, T. S., Cheng, Q., "Elastic Stiffness Properties and Behavior of Truss-Core Sandwich Panel," *Journal of Structural Engineering*, Vol. 126, No. 5, May 2000, pp 552-559.

[8]Valdevit, L., Hutchinson, J. W., Evans, A. G. (2004), "Structurally Optimized Sandwich Panels with Prismatic Cores," *International Journal of Solids and Structures*, Vol. 41, May 2004, pp. 5105-5124.

[9]Biancolini, M.E., "Evaluation of equivalent stiffness properties of corrugated board," Composite Structures, 69 (2005), 322 – 328.

[10]Buannic, N., Cartraud, P., Quesnel T., "Homogenization of corrugated core sandwich panels," Composite Structures, 59 (2003), 299 – 312.

[11]Martinez, O., Sankar, B.V., Haftka, R., Blosser, M., Bapanapalli, S.K. (2007), "Micromechanical Analysis of a Composite Corrugated-Core Sandwich Panel for Integral Thermal Protection Systems," *AIAA Journal*, 45(9), 2323-2336.

[12]Martinez, O.M., "Micromechanical analysis and design of an integrated thermal protection system for future space vehicles", PhD dissertation, University of Florida, 2007.

[13]Fung, T. C., Tan, K. H., Lok, T. S., "Analysis of C-core sandwich plate decking", Proc. 3rd International Offshore and Polar Engineering Conference, Colorado, Vol. 4, 1993, pp. 244-249.

[14]Fung, T. C., Tan, K. H., Lok, T. S., "Elastic Constants for Z-core sandwich panels," *Journal of Structural Engineering*, ASCE, Vol. 120, No. 10, 1994, pp 3046-3065.

[15]Whitney, M., *Structural Analysis of Laminated Anisotropic Plates*, Technomic, Lancaster, PA, 1987.

[16]Martinez, O., Bapanapalli, S.K., Sankar, B.V., Haftka, R.T., Blosser, M.L., "Micromechanical Analysis of Composite Truss-core Sandwich Panels for Integral Thermal Protection Systems," *47th AIAA/ASME/ASCE/AHS/ASC Structures, Structural Dynamics, and Materials Conference*, Newport, RI, May 2006.